

Optimizing the Electrode Shape for Four-electrode Electrorotation Chips

Kanokkan Maswiwat², Moritz Holtappels¹ and Jan Gimsa^{1*}

¹ Institute of Biology, University of Rostock, Gertrudenstr. 11A, 18051 Rostock, Germany.

² On leave from Department of Physics, Suratthani Rajabhat University, Amphur Muang, Suratthani 84100, Thailand.

* Corresponding author, E-mail: jan.gimsa@uni-rostock.de

Received 6 Mar 2006

Accepted 26 Jul 2006

ABSTRACT: Electrorotation experiments are conducted in harmonic rotating fields to characterize the passive electric properties of cells or particles by their frequency-dependent rotation speed. The torque of the objects is proportional to the square of the field strength. Therefore, a rotating field of constant amplitude is desirable over a large area of the measuring chamber for reproducible measurements. In this study, the field distribution in chip chambers was analyzed using numerical field simulation in combination with analytical post-processing. The electric field distribution was compared for various electrode shapes. For the center, correction factors could be calculated, relating the actual field strength to the quotient of electrode voltage and distance. Apart from the center, the field was elliptically polarized with an eccentricity increasing with the distance from the center. A spherical model object has been assumed to derive a theoretical expression for the torque induced by an elliptical field. This model allowed us to consider the torque deviation for each site with respect to the torque induced by the circular center-field. Various electrode shapes have been checked for minimum deviations of the torque. We found the optimal chip design for electrorotation to feature electrodes with round tips.

KEYWORDS: rotating fields, four-electrode chambers, electrode design, torque, cell chip.

INTRODUCTION

Electrorotation is a common technique to characterize the dielectric properties of individual cells in rotating electric fields¹⁻⁴. Cell properties can be deduced from the microscopic observation of the frequency dependence of the rotation speed induced by a rotating electric field in the frequency range from Hz to GHz. The torque leading to cell rotation is generated by the interaction of the induced cellular dipole moment with the inducing external field. Nevertheless, only the out-of-phase component of the dipole moment will contribute to the torque that is given by the cross product of the dipole moment with the external field. Mathematically, the out-of-phase component of the induced dipole is identical to its imaginary part that is different from zero only at field frequencies where electric dispersions occur. It follows that the method of electrorotation directly and sensitively detects dispersion processes, like structural (Maxwell-Wagner) and molecular (Debye) dispersions^{2,3}. The line of arguments suggests that a rotating electric field polarizing a cell translates the temporal phase shift of the induced dipole moment that would be observed in a linear field into a spatial shift leading to

cell rotation.

In classical oscilloscopes, a beam rotation, i.e. a Lissajous-circle, is generated by co-sinusoidal and sinusoidal fields applied to two electrode pairs for the x- and y- deflections. The x- and y-electrode pairs are consecutively arranged to avoid interference. Consecutive electrodes cannot be applied in electrorotation, where the field rotates in the electrode-chip plane. In four-electrode electrorotation chips, two electrode pairs simultaneously generate the two field components. As a consequence, interference has to be taken into account. It is interesting that an analogous problem exists in accelerators where the particle beam is confined by electrostatic quadrupole electrodes that are arranged around the beam-path. Optimization of their design started with complex shapes⁵ and led to four rotational rods with their symmetry axes oriented parallel to the path⁶. In the central region of the electrodes the description may be reduced to two dimensions, i.e. a plane oriented perpendicular to the beam where the accelerator-electrodes are mimicking the design of an electrorotation chip.

In electrorotation, four-electrode micro-chambers are common. To generate rotating fields, the electrodes

are driven by four sinusoidal or square-wave signals that are progressively phase-shifted by 90° ⁴. In the frequency range used for cell characterization, the electrode properties can be assumed to be linear, i.e. no frequency components other than those applied at the electrodes can evolve in the chamber. As a result, only elliptically polarized fields can be generated. The frequency spectrum of cell rotation at a frequency-independent field strengths can be analyzed to obtain dielectric properties of biological cells. For electrorotation chambers the electrode shape is an important design feature.

For a variety of electrode configurations the field distribution was analyzed by computer simulations⁷⁻¹⁰. The torque is proportional to the square of the rotating field strength^{1,8,10,11,12}. Gimsa et al.⁷ and Hölzel⁸ introduced correction factors for the field strength in chambers of different electrode designs. Hughes et al.¹⁰ considered the influence of the phase difference between the x and y components of the electric field on the torque. The torque depends on the position within the electrode chamber and the geometry of the electrodes^{9,10,13}.

In this study, we consider a sinusoidally rotating electric field in a two-dimensional chip-model for various electrode shapes using the finite element program QuickField (Tera Analysis Ltd., Denmark). The program is freely available under <http://www.quickfield.com/free.htm>. Correction factors for the various electrodes shapes were calculated for the field strength and the torque experienced by the cells. Based on these calculations; torques, acting on a spherical object at the center of chambers of different electrode designs, have been compared. For each design, the deviations of the torques relative to the distance from the center, have also been analyzed.

METHODS AND THEORY

A rotating electric field can be generated by two pairs of opposing electrodes orientated perpendicular to each other in the x-y plane. To generate a monochromatic, circular field the two pairs must be driven by co-sinusoidal and sinusoidal fields, respectively. As a result, the center-field rotates at a constant amplitude (field strength). Nevertheless, its actual amplitude can not directly be derived. Firstly, the amplitude depends on the electrode shapes. Secondly, the field strength between a pair of electrodes is also influenced by the other electrode pair of the four-electrode setup. These effects result in a reduced center field strength (E_0) deviating from the field strength calculated for a single pair of plane-parallel electrodes ($E'_0 = V/d > E_0$). We define the correction

factor of the circular field in the center as:

$$r = \frac{E_0}{E'_0} \quad (1)$$

Special cases for the chamber-field can be derived from the temporal behavior of the co-sine- and sine-functions: When one of the functions reaches its positive or negative maximum, the other is at zero amplitude. In these cases, the center field will be aligned with lines connecting (L_c) the tips of opposing electrodes, i.e. the center field vector will consecutively point at the tips of the four electrodes during one cycle (compare to Fig. 1A). The center field will be aligned with the two diagonal lines (L_d) passing in between the electrodes when the absolute values of the functions are equal (Fig. 1B). The arrow head of the field vector will describe a perfect circle when its origin is located at the center of the four-electrode chamber, for reason of symmetry. In and out of the center, the rotating field is changing from a circular to an elliptical polarization, respectively. Accordingly, the arrow heads of the field vectors will describe ellipses. When the vector-origins are located at the connecting or diagonal lines the orientations of the semi-axes of these ellipses are known: the semi-axes are aligned in parallel and perpendicular to the connecting or diagonal lines. The eccentricity of the elliptical field increases with the distance from the center.

To describe the elliptical fields we used the following simplified approach. The static electric field distributions for two phase angles, 0° and 45° , was calculated by numerical simulation with QuickField (Tera Analysis Ltd., Denmark) assuming a driving potential of 10 Vpp at an electrode tip-to-tip distance of 300 μm . The results were rescaled to 300 μm . At 0° the field strength was analyzed along the electrode tip-connecting lines L_c . These lines are orientated parallel ($L_{c\parallel}$, horizontal line in Fig. 1A connecting the positive and negative electrode) and perpendicular ($L_{c\perp}$, vertical line in Fig. 1A connecting the electrodes with zero potential) to the field. The eccentricity of an elliptical field can be derived from the maximum and minimum field strengths E_{\max} and E_{\min} , e. g. at the crossing points of $L_{c\parallel}$ and $L_{c\perp}$ with the inner circle, respectively (Fig. 1A). Since a 90° rotation of the chamber corresponds to a 90° phase progression of the field both values can be extracted from a single calculation. E_{\max} and E_{\min} determine the semi-axes of the ellipses described by the circulating vector arrow head. The analogous procedure was applied to determine E_{\max} and E_{\min} at the crossing points of the diagonal lines for a phase angle of 45° (Fig. 1B). E_{\max} and E_{\min} have been derived from values taken from the cross-points of the diagonal lines $L_{d\parallel}$ and $L_{d\perp}$ with the inner circle. As a result the field is

fully characterized at 8 points of the inner circle (Fig. 1). At the inner circle the L_c - and L_d -crossing points correspond to the shortest and the longest distances to the electrodes, respectively. Therefore, it can be assumed that the E_{max} and E_{min} values of the elliptical fields at all other points of the circle will be in between the values at these points.

The relationship between an elliptical field and the circular field in the center can be described by:

$$E_{max} = \frac{a}{r} E_0 \quad (2)$$

and

$$E_{min} = \frac{b}{r} E_0 \quad (3)$$

where a and b stand for the correction factors of

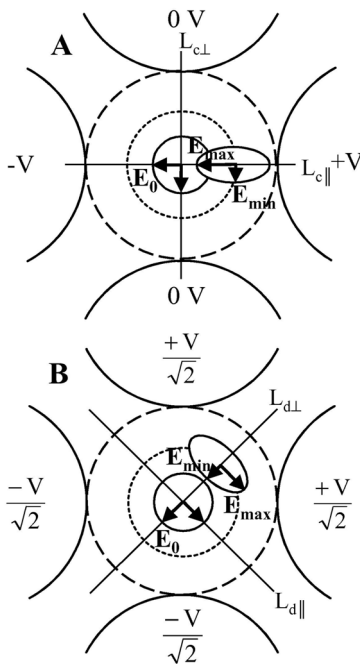


Fig 1. Sketch explaining the method of data acquisition for a chip-chamber with 300 μm electrode spacing. The long-dashed line marks the inner electrode circle with a radius of 150 μm as the reference area (see text and Table 1). The circular field in the center is described by E_0 . The elliptical fields out of the center are described by E_{max} and E_{min} . Examples for E_{max} and E_{min} at 0°- (**A**) and 45°-phases (**B**) are given (please compare to Fig.2). Plotted values were derived for a distance of 100 μm from the center (short-dashed inner circle). **A:** E_{max} and E_{min} values were derived from the crossing points of the horizontal ($L_{c\perp}$) and vertical electrode tip-connecting lines ($L_{c\parallel}$) with the inner circle (note that \parallel and \perp refer to the line orientation with respect to the field). **B:** E_{max} and E_{min} values were derived from the crossing points of diagonals $L_{d\perp}$ and $L_{d\parallel}$, respectively.

the two components of the elliptical field.

Furthermore, the eccentricity (ecc) of the elliptical field is calculated using the correction factors a and b:

$$ecc = \sqrt{1 - (b/a)^2} \quad (4)$$

Analogous to the field correction factor r it is reasonable to introduce a torque correction factor that relates E'_0 to the torque $\langle N_0 \rangle$ in the center of the chamber (for details see Appendix). Thus, the magnitude of the torque $\langle N_0 \rangle$ in the circular center field is described by:

$$\langle N_0 \rangle = r^2 E_0'^2 \text{Im}(\alpha) \quad (5)$$

where r^2 stands for the torque correction factor and $\text{Im}(\alpha)$ for the imaginary part of the polarizability of a spherical object with $\text{Im}(\alpha) = \epsilon_c \epsilon_0 V \text{Im}(\text{CMF})^9$. $\epsilon_c \epsilon_0$, V and CMF are external permittivity, volume and the Clausius Mossotti factor, respectively.

Distant from the center we find the torque $\langle N_{\text{ellip}} \rangle$:

$$\langle N_{\text{ellip}} \rangle = ab E_0'^2 \text{Im}(\alpha) = E_{max} E_{min} \text{Im}(\alpha) \quad (6)$$

with a torque correction factor of ab. Please note that in the center $ab = r^2$ for $\langle N_{\text{ellip}} \rangle = \langle N_0 \rangle$. The deviation of $\langle N_{\text{ellip}} \rangle$, ΔN_{ellip} referring to the center-torque $\langle N_0 \rangle$ is given by:

$$\Delta N_{\text{ellip}} = \frac{\langle N_{\text{ellip}} \rangle - \langle N_0 \rangle}{\langle N_0 \rangle} \quad (7)$$

We analyzed the field properties of 12 different electrode designs with squared and rounded tips by a stepwise change of electrode width D and electrode tip radius R (Table 1). The spacing d between the opposing electrode tips was kept constant at 300 μm .

RESULTS AND DISCUSSION

Electric field distribution in the rotation chamber

The field distributions for 6 different electrode designs are shown in Fig. 2. The field properties depend very much on the location within the chamber and electrode design. The field vectors in the central regions are generally homogeneous. From A to B Fig. 1 describes an anticlockwise rotation.

The electric field strength along the connecting lines $L_{c\perp}$ and $L_{c\parallel}$ and along the diagonals $L_{d\perp}$ and $L_{d\parallel}$ is plotted in Fig. 3 (please note, that Figs. 4A and B are zoom-plots of Figs. 3A and C). For any distance from the center the two components of the elliptical field, E_{max} and E_{min} , were derived along the L_c and L_d lines. At phase 0° values of E_{max} were found along line $L_{c\perp}$. Values

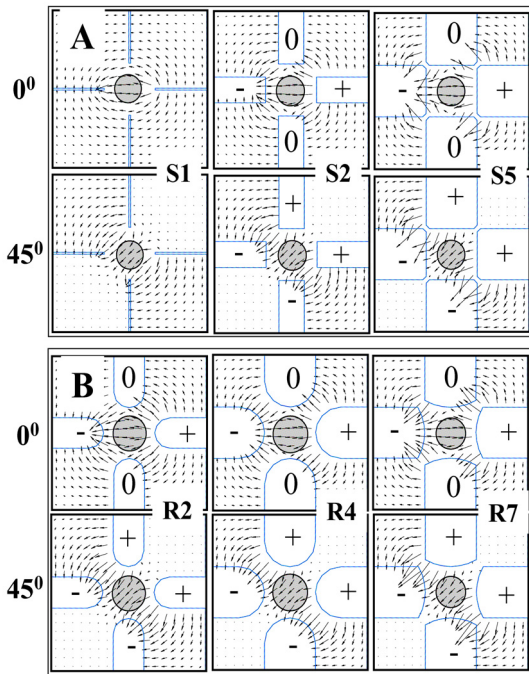


Fig 2. Distribution of the electric field strength in the x-y plane of different electrode chambers (Table 1) driven by 0°- and 45°- phase signals. **A:** squared electrodes S1, S2 and S5. **B:** rounded tip electrodes R2, R4 and R7. The arrows are vectors of the electric field strength. The circular areas with torque deviations below 10% are marked in gray. Their radii were determined from the minima of the $S_{10\%}$ -values along the connecting and diagonal lines marked by an asterisk in Table 1.

of E_{\min} were found along line $L_{c\perp}$. At phase 45°, E_{\max} and E_{\min} values were found along lines $L_{d\parallel}$ and $L_{d\perp}$, respectively.

For all electrode designs the field strength in the center varies between 24 and 28 kV/m, i.e. 73% - 84% of E'_0 . Distant from the center, the performance of the square- and round-tipped electrodes is qualitatively different. There, the field strength for squared electrodes is either below (at line $L_{c\parallel}$) or above (at line $L_{d\parallel}$) the field strength of the round-tip electrodes. For both shapes the field eccentricity increases with the distance from the center. It varies from 0 (circular field) at the center to about 0.95 (extremely flattened ellipse) at a distance of 120 μm (Fig. 5). The increasing eccentricity seems to be independent from the electrode design. Only square-tipped electrodes (Fig. 5B) show different eccentricities along the diagonal lines $L_{d\perp}$.

Torque correction factors at the center and at sites distant from the center

The field strengths at the center of various rotation chambers are related to the torque correction factor r^2 that is presented in relation to the electrode

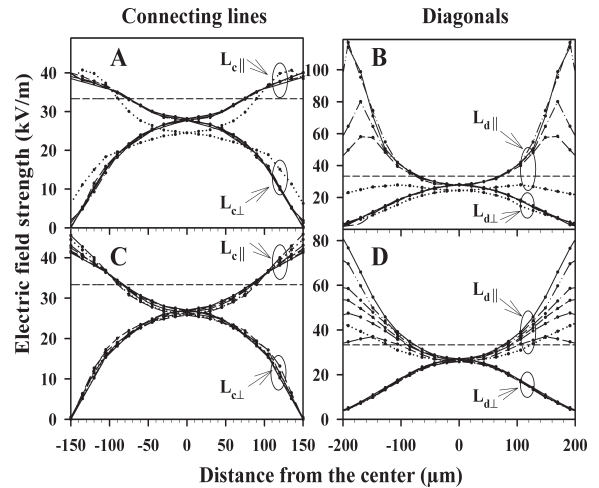


Fig 3. Field strength variation along the connecting lines $L_{c\perp}$ and $L_{c\parallel}$ and the two diagonals $L_{d\perp}$ and $L_{d\parallel}$. **A** and **B** show the electric field strength for the squared electrodes: S1 (dot), S2 (short dash), S3 (dash dot), S4 (dash dot-dot), and S5 (solid). **C** and **D** show the electric field strength of the of rounded tip electrodes: R1 (medium dash), R2 (dot), R3 (long dash), R4 (short dash), R5 (dash dot), R6 (dash dot-dot) and R7 (solid). The straight-dashed line marks the field strength of $E'_0=33.3$ kV/m that would be observed in between a pair of plane parallel electrodes.



Fig 4. A: Zoom of Fig. 3A, **B:** zoom of Fig. 3C. For symbols see Fig. 3.

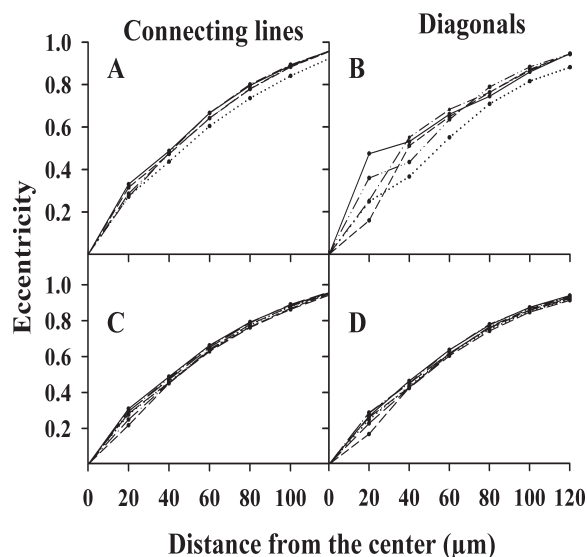


Fig 5. The eccentricity of the electric field as a function of the distance from the center for squared electrodes (A and B) and rounded tip electrodes (C and D). For symbols see Fig. 3.

characteristics D/d and R/d in Table 1. For r^2 a maximum in the range from 66% to 71% of N'_0 was found for ratios of D/d and R/d above 0.5. Above these ratios r^2 remains fairly constant and a change in electrode width does not further affect the center field whereas r^2 decreases for ratios below 0.5. For the pin electrodes (S1) r^2 is smallest. Comparing the round- and square-tipped electrodes with a ratio above 0.5, the latter show slightly higher values for r^2 .

Table 1. Designs of various electrode chambers. For all chambers the spacing d between the electrode tips was 300 μm. Electrode characteristics D/d and R/d (D , R and d stand for electrode width, electrode tip radius and spacing between electrodes, respectively), torque correction factor r^2 and distance from the center at which the torque reaches a deviation of 10% ($S_{10\%}$) along the connecting and diagonal lines. The last column presents the relative area with respect to the inner electrode circle with a radius of 150 μm (see Fig. 1) inside which the torque deviation is below 10%. The circular areas were determined from the minima of the $S_{10\%}$ -values along the connecting lines (L_c) and the diagonals (L_d) marked by an asterisk (see Fig. 2).

Shape	Designs	Width D (μm)	Radius R (μm)	D/d(squared electrodes) R/d(rounded tip electrodes)	r^2	$S_{10\%}$ in μm		% of usable area
						L_c	L_d	
Square	S1	10	-	0.03	0.54	84	76*	25.67
	S2	150	-	0.5	0.71	80.5*	110	28.80
	S3	180	-	0.6	0.70	77*	>120	26.35
	S4	240	-	0.8	0.69	82*	>120	29.88
	S5	300	-	1.0	0.71	77.5*	>120	26.69
Round	R1	150	75	0.25	0.60	108	93*	38.44
	R2	180	90	0.3	0.61	99	94*	39.27
	R3	240	120	0.4	0.63	88*	100	34.41
	R4	300	150	0.5	0.65	99*	99*	43.56
	R5	300	180	0.6	0.66	85*	104	32.11
	R6	300	240	0.8	0.65	85*	112	32.11
	R7	300	300	1.0	0.66	84*	115	31.36

An important criterion for the usability of an electrorotation chamber is the torque deviation inside the measuring volume of the chamber. In a plane chip this volume is confined to an area with comparable torques. We defined circular areas by allowing for a torque deviation up to 10% with respect to the torque in the center. Along the L_c and L_d -lines $S_{10\%}$ -distances were defined by the points with a torque-deviation of 10%. The radius of the experimentally usable area was

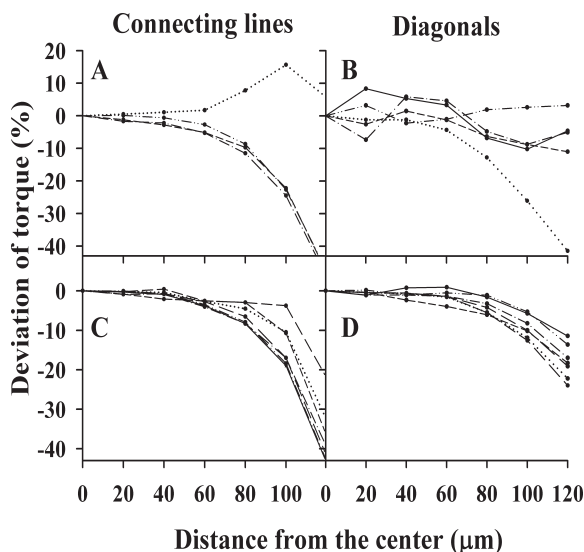


Fig 6. Distance dependence of the torque deviation along connecting lines and diagonals. A and B: squared electrodes. C and D: rounded tip electrodes. For symbols see Fig. 3.

calculated from the minimum of the two $S_{10\%}$ -distances. The results are given in Table 1 and displayed by the grayish circles in Fig. 2. For all electrode designs the minimum of the $S_{10\%}$ -distances was at least $75\ \mu\text{m}$ (Fig. 6). With the exception of electrode design S1, $S_{10\%}$ along the diagonal lines (Figs. 6B and D) was always larger ($90\text{--}100\ \mu\text{m}$) than $S_{10\%}$ along the connecting lines (around $80\ \mu\text{m}$, Figs. 6A and C). Furthermore, the torque for the square-tipped electrodes shows an undulating pattern (Fig. 6B) contrasting the obvious decrease of torque of the round-tipped electrodes (Fig. 6D). Nevertheless, we believe that the undulations result from the limited capacity of the software.

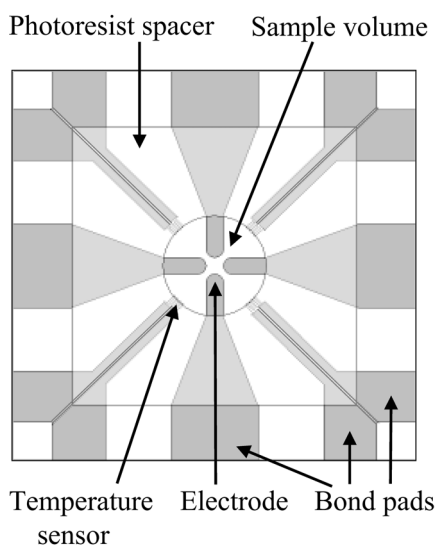


Fig 7. Scheme of our new glass electrorotation chips with platinum electrodes of design R4. The radius of the electrode tip is $150\ \mu\text{m}$. The width of the electrode and the spacing are $300\ \mu\text{m}$. Temperature sensors have been processed from a platinum meander-structure to follow temperature changes in the chamber. A photoresist structure forms the side walls limiting the sample volume that is confined by a cover slip during measurements.

A summary of the electrode properties is given in Table 1. At first sight, r^2 as well as $S_{10\%}$ are similar amongst the round-tipped electrode designs, whereas the square-tipped electrodes show higher differences in $S_{10\%}$ along the connecting and diagonal lines. Although $S_{10\%}$ along the diagonal lines for the square-tipped electrodes is very high, these electrodes are less appropriate since the low $S_{10\%}$ along the connecting line is limiting the useable chip area. Additionally, the square-tipped electrodes generate extremely high field strengths at their sharp edges. This may lead to particle collection at the edges due to dielectrophoretic effects. Amongst the round-tipped electrodes, a maximum area of constant torque is found for the design R4. In this

design $S_{10\%}$ is about $100\ \mu\text{m}$ along both the connecting and diagonal lines. Therefore, out of 12 analyzed electrode designs, R4 was chosen for use in the new chip designs (Fig. 7, produced by GeSiM GmbH, Grosserkmannsdorf, Germany).

CONCLUSION

Numerical simulations with a freely available software for electrostatic fields yields valuable information on the quality of rotating fields in electrorotation chip-chambers when combined with a simple analytical post-processing. The field strength and torque correction factors introduced provide a basis for comparing experimental results obtained with chambers of different electrode designs. The maximum field strength in the center of 4-electrode rotation chambers never exceeds 85% of the field strength generated by a single pair of equi-planar electrodes. Furthermore, we could determine the site dependence of the torques experienced by spherical objects within the electrorotation-chips. These considerations allowed us to specify the electrode-chips with the largest areas of a torque deviation below 10% amongst all considered designs. It has a round-tipped electrode with $R/d = 0.5$. There are a number of alternative electrode shapes that have not been considered in this study such as pyramidal or hyperbolic shapes. Furthermore, this approach can be a useful tool not only for planar 4-electrode chambers but also for other planar designs of central symmetry, like 3, 6, or 8-electrode chambers. Probably, it can also be applied in 3-dimensional designs like those used in micro-fluidic lab-on-chip devices.

ACKNOWLEDGMENTS

K.M. is grateful for a stipend from the Royal Thai government. Dr. H.-W. Glock and D. Wachner are acknowledged for helpful discussions. This study has partly been supported by grant StSch 20020418A of the Bundesamt für Strahlenschutz to J.G. The authors are grateful to the International Postgraduate Programmes (IPP) supported by DAAD, BMBF and DFG.

REFERENCES

1. Gimsa J, Glaser R and Fuhr G (1991) Theory and application of the rotation of biological cells in rotating electric fields (Electrorotation). In: *Physical characterization of biological cells* (Edited by Schütt W, Klinkmann H, Lamprecht I and Wilson T), pp 295–323. Verlag Gesundheit GmbH, Berlin.
2. Gimsa J (2001) A comprehensive approach to electro-orientation, electrodeformation, dielectrophoresis, and electrorotation of ellipsoidal particles and biological cells. *Bioelectrochem* 54, 23–31.

3. Jones TB (1995) *Electromechanics of particles*. Cambridge University Press, USA.
4. Gimsa J, Müller T, Schelle T and Fuhr G (1996) Dielectric spectroscopy of single human erythrocytes at physiological ionic strength: Dispersion of the cytoplasm. *Biophys J* **71**, 495-506.
5. Stokes RH, Crandall KR, Stovall JE and Swenson DA (1979) RF Quadrupole Beam Dynamics. *IEEE Trans Nuc Sci* **NS26**, 3469-79.
6. Junior P, Deitinghoff H, Halfmann KD, Neumann W and Zoubek N (1983) Design Considerations on Peak Electrical Fields and Maximum Beam Currents for Heavy Ion RFQ Linacs. *IEEE Trans Nuc Sci* **NS30**, 2639-41.
7. Gimsa J, Glaser R and Fuhr G (1988) Remarks on the field distribution in four electrode chambers for electrorotational measurements. *Studia biophysica* **125**, 71-6.
8. Hölzel R (1993) Electric field calculation for electrorotation electrodes. *J Phys D: Appl Phys* **26**, 2112-6.
9. Hughes MP (1998) Computer-aided analysis of conditions for optimizing practical electrorotation. *Phys Med Biol* **43**, 3639-48.
10. Hughes MP, Wang X-B, Becker FF, Gascoyne PRC and Pethig R (1994) Computer-aided analyses of electric fields used in electrorotation studies. *J Phys D: Appl Phys* **27**, 1564-70.
11. Lampa A (1906) Über Rotation im electrostatischen Drehfelde. *Wiener Berichte* **115**, 1659-90.
12. Schwan HP (1988) Dielectric spectroscopy and electro-rotation of biological cells. *Ferroelectrics* **86**, 205-23.
13. Hughes MP, Archer S and Morgan H (1999) Mapping the electrorotational torque in planar microelectrodes. *J Phys D: Appl Phys* **32**, 1548-52.

APPENDIX

Torques acting on objects at different sites of the measuring area

The time average torque in circularly polarized fields,

$$\langle \vec{N} \rangle = \frac{1}{2} \text{Re} [\vec{m} \times \vec{E}^*] \tag{A1}$$

is given by the cross-product of the induced dipole moment (\vec{m}) and the conjugated field (\vec{E}^*)^{2,3}. The elliptical AC field in the x-y plane can be written in component notation as (see Fig. 1, Eqs. (2) and (3)):

$$\vec{E} = \begin{pmatrix} E_x \\ E_y \\ E_z \end{pmatrix} = \begin{pmatrix} a/r & E_0 \\ j & b/r & E_0 \\ 0 \end{pmatrix} = \begin{pmatrix} E_{\max} \\ E_{\min} \\ 0 \end{pmatrix} \tag{A2}$$

Both, the x- and y- field components are sinusoidal with a 90°-phase shift, denoted by $j = \sqrt{-1}$. We assume that the magnitude of the field component oriented in \hat{i} -direction is larger than in \hat{j} -direction with no limitation in generality. For the elliptical field apart from the center,

factors a and b were introduced leading to:

$$E_{\min} = j \frac{b}{a} E_{\max} \tag{A3}$$

and the conjugated fields:

$$E_{\min}^* = -j \frac{b}{a} E_{\max}^* \tag{A4}$$

(see Eqs. (2) and (3)). The induced dipole moment \vec{m} is proportional to the field. In component notation \vec{m} is given by⁹:

$$\vec{m} = (m_x \quad m_y \quad m_z) = (\alpha E_{\max} \quad \alpha E_{\min} \quad 0) \tag{A5}$$

Introducing Eqs. (A2) and (A5) the torque of Eq. (A1) becomes:

$$\langle \vec{N} \rangle = \frac{1}{2} \text{Re} (\alpha E_{\max} E_{\min}^* - \alpha E_{\min} E_{\max}^*) \hat{k} \tag{A6}$$

where \hat{k} stands for the unit vector pointing in z-direction. Introducing Eq. (A4) we get:

$$\langle \vec{N} \rangle = \frac{1}{2} \text{Re} \left(\alpha \left(E_{\max} \left(-j \frac{b}{a} \right) E_{\max}^* - E_{\min} \left(j \frac{a}{b} \right) E_{\min}^* \right) \right) \hat{k} \tag{A7}$$

Eq. (A7) can re-written as:

$$\langle \vec{N} \rangle = \frac{1}{2} \text{Im} \left(-j \alpha \left(E_{\max}^2 \left(\frac{b}{a} \right) + E_{\min}^2 \left(\frac{a}{b} \right) \right) \right) \hat{k} \tag{A8}$$

Introducing Eqs. (2) and (3) for E_{\max} and E_{\min} we obtain:

$$\langle \vec{N} \rangle = \left(\frac{ab}{r^2} \right) E_0^2 \text{Re} (-j \alpha) \hat{k} \tag{A9}$$

which can be simplified to:

$$\langle \vec{N} \rangle = \left(\frac{ab}{r^2} \right) E_0^2 \text{Im}(\alpha) \hat{k} \tag{A10}$$

Accordingly, the torque in an elliptical field is:

$$\langle \vec{N} \rangle = E_{\max} E_{\min} \text{Im}(\alpha) \hat{k} \tag{A11}$$

and reduces to:

$$\langle \vec{N} \rangle = E_0^2 \text{Im}(\alpha) \hat{k} \tag{A12}$$

in a circular field with $r = a = b$.